Tellus (1999), 51A, 289–303
Printed in UK – all rights reserved

TELLUS
ISSN 0280–6495

Alpine precipitation in a tripled CO_2-climate

By ULRIKE BURKHARDT*, [1]*Meteorologisches Institut, Universität München, Theresienstr. 37, 80333 München, Germany*

(Manuscript received 6 October 1997; in final form 29 June 1998)

ABSTRACT

A statistical model is constructed to determine the change in wintertime monthly mean Alpine precipitation due to a tripling of the CO_2 concentration. The model is based on optimally correlated pairs of predictand (Alpine precipitation) and predictor (500 hPa geopotential) patterns which were determined from observational data by a canonical correlation analysis. The statistical model is applied to the change in large scale climate simulated by a general circulation model (GCM) for a $3 \times CO_2$ concentration. The statistical model predicts a change of Alpine precipitation of up to 6% of the observed monthly rainfall for a $3 \times CO_2$ climate. A maximal increase of wintertime precipitation is obtained for the stations in the south of the Alps and only slight changes are predicted for the stations in the north of the Alps. It is found to be important to remove the area averaged change of the geopotential simulated by the GCM and to apply the statistical model only to the spatial variation of the geopotential. The regional climate change estimated with the statistical model depends only slightly on the exact set-up of the model. Thus the error of the statistical model seems to be small in comparison with the uncertainty in the large scale climate predicted by the GCM for $3 \times CO_2$ conditions.

1. Introduction

The best estimates of the large scale climate change due to an increasing CO_2 concentration are provided by general circulation model (GCM) simulations. On the regional scale these climate simulations are very unreliable (Grotch and McCracken, 1991). In particular, the effect of small scale forcings, such as complicated orography and coastlines, can not be captured by the GCMs (Giorgi and Mearns, 1991). A prime example of such a small scale forcing in Europe is provided by the Alps. But since it is especially the regional scale climate change which is needed for climate impact studies, a regional interpretation of the GCM simulations is necessary. Therefore, in this study, the large scale simulations of a GCM are regionalized with regard to the precipitation in the area of the Alps. Precipitation was chosen because it is an important variable for climate impact studies and since there has been little progress detectable in the simulation of precipitation (Boer et al., 1992) even by the more recent and higher resolution GCMs (Cubasch et al., 1996).

Several methods for the regionalization of GCM climate change scenarios have been developed (Giorgi and Mearns, 1991). These regionalization methods all rely on a successful simulation of the large scale climate by the GCMs (which is commonly inferred from their skill in simulating present day climate), from which the change in the small scale climate is inferred. One class of methods uses a regional model which is nested into the GCM simulations (Giorgi, 1990; Giorgi et al., 1990; Marinucci and Giorgi, 1992; Giorgi et al., 1992; Marinucci et al., 1994; Jones et al., 1997), or a regional model that is connected to the GCM simulations in a statistical way (Frey-

* Current affiliation: Department of Meteorology, University of Reading, 2 Earley Gate, Reading, RG6 6BB, UK.

Buness et al., 1995; Egger, 1995). A 2nd group of methods uses statistical models to infer the regional climate from the large scale climate. These may use weather patterns, sometimes combined with stochastic models for the construction of daily scenarios (Hughes et al., 1993; Bardossy and Plate, 1992; Saunders and Byrne, 1996), or may be based on multivariate regression models (Kim et al., 1984; Karl et al., 1990; Von Storch et al., 1993; Gyalistras et al., 1994).

The nesting of regional models into GCM simulations is computationally very intensive since the resolution of the regional model has to be high enough to ensure that the effects of regional scale forcings are captured, and since the model domain has to be big enough that the circulation in the regional model is not completely dominated by the forcing by the global model (Machenhauer et al., 1996). Therefore this method has often been tested in the simulation of particular episodes or short data sets (Giorgi et al., 1990; Marinucci and Giorgi, 1992). Problems with the regional models may occur, due to the assumption that parameterizations still hold in a changed climate, and due to the poor determination of land use distribution. Nevertheless, this method is often, but not always, successful (Marinucci et al., 1994, Machenhauer et al., 1996). Because of the large amount of computing time needed for regional models and because of the uncertainties that still exist with these methods, a statistical model was chosen for the present regionalisation study.

Statistical models use the statistical relationships between the large scale and the small scale climate found in observational data. If those relationships are strong then the statistical model can infer a high percentage of the variability of the small scale field from the large scale field. In using those relationships for the regionalization of the simulated large scale climate change, it is assumed that the relationships will stay the same in a changed climate.

In this paper, the change of the Alpine precipitation due to a tripling of the CO_2 concentration is derived from the large scale simulations of the ECHAM3/T42 model (Perlwitz et al., 1993). In order to do that, a multivariate regression model is constructed which relates the Alpine precipitation (predictand) to the large scale 500 hPa height field (predictor). The regression model is here based on statistical relationships between the predictand and predictor data set found in observational data. Those relationships can be found using a Canonical Correlation Analysis (CCA), as in Von Storch et al. (1993), which determines the patterns of the predictor and predictand data sets which are optimally correlated in time. The relationship between the 2 fields used in this study in observations and model simulations has been discussed already in an earlier paper (Burkhardt, 1995). It should be noted that CCA is only able to pick up the linear relationships between the 2 different fields. Especially when dealing with daily data, nonlinearities in the connection between different fields can be very important, suggesting that methods such as neural networks are of interest (Hewitson and Crane, 1992, McGinnis, 1997).

When deducing the change in local climate from the change in the large scale circulation only, it must be assumed that this is the most important cause for a change in local climate. This will hold most strongly in areas with strong mesoscale forcing such as the Alps (Jones et al., 1997). Nevertheless, it should be kept in mind that such a statistical model disregards the effect that a change in water vapour or other variables will have on the precipitation in a climate with increased CO_2 concentration.

In Section 2 the data and the methodology are described. In Section 3 the relationship between the observed fields of large scale 500 hPa geopotential height and Alpine precipitation is analysed using a CCA. Different setups of a multivariate regression model are formulated using the results of the CCA of the observational data and validated on an independent time series (Section 4). In Section 5, the quality of the GCM simulation of the predictor field is examined using an EOF Analysis and the regression model is applied to the change of the large scale 500 hPa geopotential height field simulated by the GCM for a $3 \times CO_2$ concentration. The precipitation change simulated directly by the GCM and inferred from the large scale GCM simulations by the statistical model are compared. Finally, in Section 6, the change of precipitation estimated by this study are compared with estimates made in other studies.

2. Data and methodology

2.1. Observational data

A statistical model is constructed using the results of a statistical analysis of observational

Table 1. *Rainfall measuring stations and their mean wintertime precipitation. The country in which the stations lie are indicated in brackets with F standing for France, G for Germany, S for Switzerland, I for Italy and A for Austria*

Station	Latitude	Longitude	Precipitation (mm/month)
Dijon (F)	47.3	5.1	57
Geisenheim (G)	50.0	8.0	42
Geneve (S)	46.1	6.1	69
Hohenpeißenberg (G)	47.8	11.0	67
Milano (I)	45.5	9.2	59
München (G)	48.1	11.7	55
Nancy (F)	48.7	6.2	62
Salzburg (A)	47.8	13.0	67
Sonnenblick (A)	47.1	13.0	115
Strasbourg (F)	48.6	7.6	35
St. Pölten (A)	48.2	15.6	39
Trieste (I)	45.7	13.8	74
Venezia (I)	45.4	12.4	59
Wien (A)	48.3	16.4	39
Zugspitze (G)	47.4	11.0	172
Zürich (S)	47.2	8.3	77

data. The observational data used are monthly mean values of precipitation and 500 hPa geopotential height for the winter months (December-February). The 500 hPa field was used instead of the surface pressure field, which would have been available for a much longer period, since CCA showed that the surface pressure field is not as strongly connected with the precipitation as the 500 hPa height field. The observational data consist of the NMC analysis of 500 hPa geopotential heights (on a $5.6^\circ \times 5.6^\circ$ grid), and precipitation data from 16 stations located in or close to the Alps (Table 1), for the years 1951–1984. The station data were obtained from the World Meteorological Station Climatology (WMSC) and the European Meteorological Station Data (EMSD).

2.2. CCA

The method of canonical correlation analysis is used in this study. CCA, like EOF analysis, is a coordinate transformation determining the maximum correlations in 2 data sets ($\boldsymbol{X}$ and $\boldsymbol{Y}$). Before applying CCA to the data, the data fields are filtered by an EOF-analysis (Barnett and Preisendorfer, 1987; Bretherton et al., 1992). This filtering retains a limited number of degrees of freedom explaining most of the variance, and eliminates noise and some small-scale features of the data. Here the EOFs of both geopotential and precipitation were determined using the cross correlation matrix in order to suppress the influence of the Alpine stations which would dominate the EOFs because of their large precipitation variance. CCA calculates coefficients $s_k^{(i)}$ and $t_k^{(i)}$, so that the linear combinations of the first F_x and F_y EOF-time series ($a_k(t)$ and $b_k(t)$) of the 2 data sets

$$u^{(i)}(t) = \sum_{k=1}^{F_x} s_k^{(i)} \cdot a_k(t), \qquad v^{(i)}(t) = \sum_{k=1}^{F_x} t_k^{(i)} \cdot b_k(t), \tag{1}$$

are most highly correlated. This correlation is called the canonical correlation, $\rho^{(i)}$. When a pair of maximally correlated time series (indicated by the superscript i) is found, the next pair $(i+1)$ is calculated under the additional constraint that their time series are uncorrelated with the time series of the earlier patterns. The covariance between the time series $u^{(i)}(t)$ and $v^{(i)}(t)$ and the original non-normalized data sets yields a pair of patterns $\boldsymbol{g}^{(i)}(t)$ and $\boldsymbol{h}^{(i)}(t)$, which contain the variance of the original field. It is those fields which will be shown and discussed in the following. CCA is described in detail by Anderson (1984) and Preisendorfer (1988) and has been applied successfully in atmospheric and oceanic science (Barnett and Preisendorfer 1987; Metz 1991).

2.3. Significance testing

The results of the CCA were tested for significance. Following Metz (1991) the significance of the canonical correlations was tested using a Monte-Carlo method. Random time series were obtained by a Markov model and analysed by a CCA in place of the EOF time series of the observational data. The random time series were constructed to account for the red noise character of the EOF time series. The canonical correlations obtained by the CCA of 100 different sets of random time series were ordered by their value and the level over which 5% or 1% of the correlations lie is determined. The canonical correlations are judged significant on a 95% or 99% level if they are higher than these significance levels.

There are 2 potential problems with this kind of significance test. The first is connected with the non-normal distribution of the precipitation data. With the Markov model time series have been constructed which are normally distributed whereas the EOFs of the monthly mean precipitation data may be slightly non-normally distributed. This can introduce a bias in the significance levels and, as suggested by Wilks (1995), a bootstrap method may possibly be preferable. The 2nd potential problem is that the timeseries generated by the Markov model are numerically not exactly uncorrelated. The application of an EOF-Analysis to these time series would provide numerically uncorrelated time series which could then be analysed by the CCA. This 2nd effect is likely to change the significance levels only marginally. Nevertheless, the skill of the model based on the results of the CCA (see next paragraph) described in Section 4 confirm the results of the significance analysis in Section 3. This indicates that the two problems described above do not strongly influence the significance testing carried out in this study.

2.4 *Regression model*

The results of the CCA are used in order to construct a multivariate regression model (similar to that of Von Storch et al., 1993), which estimates the Alpine precipitation (predictand) from the large scale 500 hPa geopotential height field (predictor). The regression model describes the part of the precipitation field, $\boldsymbol{x}$, which can be described by the predictand patterns, $\boldsymbol{g}^{(i)}$,

$$\boldsymbol{x}'(t) \approx \sum_{i=1}^{M} u^{(i)}(t)\boldsymbol{g}^{(i)} \approx \sum_{i=1}^{M} \rho^{(i)} v^{(i)}(t)\boldsymbol{g}^{(i)} = \hat{\boldsymbol{x}}'(t), \tag{2}$$

with $\boldsymbol{x}'$ being the time anomaly of $\boldsymbol{x}$, $\hat{\boldsymbol{x}}'$ the approximation of this time anomaly and M the number of canonical correlation patterns used for the approximation. The amplitude of the predictand patterns, $u^{(i)}(t)$, is approximated by the amplitude of the associated predictor pattern, $v^{(i)}(t)$ (both amplitude time series have unit variance), multiplied by the canonical correlation. The time series $v^{(i)}(t)$ is determined by projecting the geopotential field onto the EOF patterns of the geopotential and using eq. (1). The amount of the variance of the precipitation field that can be estimated from the geopotential field depends on the canonical correlation, $\rho^{(i)}$, which is the maximal correlation between any two time series of patterns of the two fields, and on the amount of variance described by the homogenous covariance pattern, $\boldsymbol{g}^{(i)}$.

In order to validate the regression model the time series of the data sets are split into two halves and the regression model is constructed using an analysis of only one half of the time series. The regression model is applied to the geopotential data to estimate the precipitation field which is then compared with the observed precipitation. The skill

$$S = 100\left(1 - \frac{\langle(\boldsymbol{x}' - \hat{\boldsymbol{x}}')^2\rangle}{\langle \boldsymbol{x}'^2 \rangle}\right), \tag{3}$$

with $\langle .. \rangle$ denoting a time average, is a measure of the performance of the regression model.

2.5. *GCM data*

After examining how realistically the predictor field is simulated by the GCM in a simulation of the present climate ($1 \times CO_2$), the statistical model is applied to GCM simulations with an increased CO_2 concentration ($3 \times CO_2$). ECHAM3/T42 model data (Roeckner et al., 1992; DKRZ Modellbetreuungsgruppe, 1994) for precipitation ($2.8^\circ \times 2.8^\circ$ grid) and 500 hPa geopotential height (resolution reduced to $5.6^\circ \times 5.6^\circ$) were obtained from two simulations. One is a $1 \times CO_2$ and the other a $3 \times CO_2$ experiment, both 30 years long. The simulations are time slice experiments (Perlwitz et al., 1992). This means that the seasonal cycle of the surface temperature of the ocean is prescribed. For the $3 \times CO_2$ experiment this seasonal cycle consists of the change of the SST due to a tripling of CO_2 which is simulated after about 100 years in an IPCC Scenario A experiment with the ECHAM1/LSG model (Cubasch et al., 1992) plus the mean seasonal cycle. The ECHAM3/T42 time slice experiments are used since this version of the model simulates the large scale climate much more realistically than the older ECHAM1-version (Roeckner et al., 1992), which has frequently been used for regionalisation studies.

3. Relationship between the precipitation field and the pressure field

A CCA between the observed precipitation field and the observed field of the 500 hPa height (in the area bounded by 40°N and 60°N and 15°W and 20°E, i.e., western Europe) is performed after filtering the data by an EOF-analysis following Barnett and Preisendorfer (1987).

It is crucial to determine the optimal number of EOFs retained for the CCA. On the one hand it is necessary to exclude those EOF-time series which do not increase the canonical correlation significantly and to keep down the level that the correlations must exceed to be regarded as significant; on the other hand a strong filtering could mean that some information about the relation of the 2 fields is filtered out. To identify the optimal number of EOFs, that is the optimal truncation point, the CCA was carried out including a varying number of EOFs of both fields. Table 2 contains the canonical correlations, their significances and the amount of variance explained by the precipitation pattern.

There are up to 4 canonical correlations which are significant at the 99% level. It can be seen that for any given number of time series of precipitation EOFs used, the canonical correlations increase when the time series of 2 instead of one EOF of the geopotential are used. Inclusion of the time series of the 3rd EOF of the geopotential in the CCA causes, on the one hand, the 2nd highest canonical correlation to grow and, on the other hand, a rise in variance described by the precipitation pattern which is connected with the highest canonical correlation. The use of more than the time series of the first 3 EOFs of the geopotential field results in only slightly higher canonical correlations and about the same amount of described precipitation variance. The use of more than 4 time series of the EOFs of the precipitation field causes the correlations to rise and the variance described by the precipitation pattern to decrease. The use of more than 3 or 4 EOFs of each field is therefore not necessary.

Since the inclusion of the time series of more than 2 EOFs of the precipitation field in the CCA yields only slightly higher canonical correlations and precipitation variances, the inclusion of the time series of more than 2 EOFs for the CCA is actually not necessary. However, this would mean that the information about the precipitation at the Austrian stations would hardly be included in the subsequent analysis since the first 2 EOFs of the precipitation field explain very little of the variance at these stations. Therefore the CCA was performed including the time series of the first 4 EOFs of the precipitation and the first 3 EOFs of the 500 hPa geopotential height field. The first 3 EOFs of the large scale field of the 500 hPa geopotential height field explain 90% of the variability of the field (Table 2). Multiplied with a positive (negative) amplitude the first 3 EOFs describe the following pressure anomalies respectively:

- a high (low) pressure anomaly in the middle of the analysed area;
- a southwest (northeast) wind anomaly;
- an enhanced (weakened) approximately zonal flow, with the geopotential gradient directed from west-northwest to east-southeast (from east-southeast to west-northwest).

The first 4 EOFs of the precipitation field describe 81% of the variance (Table 2) and in connection with a positive (negative) amplitude then describe:

- positive (negative) precipitation anomalies which are maximal north and west of the Alps;
- small positive (negative) anomalies in the northeast and negative (positive) anomalies in the south and west of the Alps;
- positive (negative) anomalies in the south and east of the Alps and negative (positive) anomalies in the northwest;
- smaller scale precipitation anomalies which have a relatively large amplitude at the eastern and Alpine stations.

The CCA of the time series of these first 3 EOFs of the 500 hPa geopotential height field and the first 4 EOFs of the precipitation field yields 3 significant canonical correlations. Most highly correlated is a pair of patterns which describes a predominantly westerly flow anomaly which is connected with positive precipitation anomalies at each station (Fig. 1). The pair of patterns can be interpreted with both signs, as follows. The anomalous geopotential pattern and the mean geopotential height would add up to give enhanced westerlies (not shown). These enhanced westerlies are associated with the rainfall anomalies shown in Fig. 1b. On the other hand subtraction of the geopotential anomaly pattern from the time mean

Table 2. *Canonical correlations and variance described by the canonical precipitation pattern (in percent) depending on the number of EOFs used for the analysis*

Number coef.	Geop. →	1		2		3		4		5		6	
precip. ↓	Cumu. variance	50.0		76.1		90.0		94.9		97.8		98.7	
1	50.0	0.47 ∗	50.0	0.72 ∗	50.0	0.87 ∗	50.0	0.87 ∗	50.0	0.88 ∗	50.0	0.90 ∗	50.0
2	65.1	0.61 ∗	36.0	0.85 ∗ 0.09	39.4 25.7	0.87 ∗ 0.73 ∗	47.7 17.4	0.87 ∗ 0.76 ∗	48.5 16.6	0.88 ∗ 0.78 ∗	49.4 15.8	0.9 ∗ 0.78 ∗	48.8 16.3
3	75.0	0.61 ∗	35.8	0.85 ∗ 0.15	39.3 14.4	0.88 ∗ 0.74 ∗ 0.10	47.8 16.6 10.7	0.88 ∗ 0.77 ∗ 0.16 ○	48.5 15.5 11.0	0.89 ∗ 0.79 ∗ 0.18	49.0 15.2 10.9	0.92 ∗ 0.79 ∗ 0.23	48.2 15.4 11.4
4	80.7	0.61 ∗	35.4	0.85 ∗ 0.16	39.3 13.1	0.88 ∗ 0.74 ∗ 0.13 ○	47.7 16.6 9.1	0.88 ∗ 0.77 ∗ 0.16 0.10	48.5 15.5 11.0 5.7	0.89 ∗ 0.79 ∗ 0.23 0.16	48.8 15.1 6.5 10.3	0.92 ∗ 0.79 ∗ 0.37 0.16	48.2 15.4 7.1 10.1
5	85.6	0.63 ∗	34.1	0.86 ∗ 0.20	39.1 11.2	0.88 ∗ 0.77 ∗ 0.15	48.0 15.1 8.8	0.88 ∗ 0.78 ∗ 0.45 ∗ 0.14	48.5 15.1 5.4 9.8	0.89 ∗ 0.81 ∗ 0.49 ∗ 0.22 0.12	48.5 14.4 6.0 5.9 10.7	0.92 ∗ 0.81 ∗ 0.50 ∗ 0.35 ∗ 0.12	48.3 14.3 6.2 6.3 10.4
6	89.2	0.63 ∗	34.1	0.86 ∗ 0.21	38.5 10.2	0.88 ∗ 0.85 ∗ 0.18	47.2 13.6 6.6	0.89 ∗ 0.85 ∗ 0.51 ∗ 0.18	47.7 13.3 6.8 6.6	0.9 ∗ 0.85 ∗ 0.52 ∗ 0.37 ∗ 0.17 ○	44.0 17.1 7.0 4.6 7.5	0.92 ∗ 0.86 ∗ 0.52 ∗ 0.45 ∗ 0.24 ○ 0.01	47.2 13.4 6.9 5.7 6.8 9.1

The 1st row and column list the number of EOFs of the respective fields used in the CCA, and the 2nd row and column give the cumulative percentage of the variance explained by those EOFs. In each square are given the canonical correlations (on the left side) and the variance described by the precipitation pattern (right side) of all canonical correlation patterns resulting from a canonical correlation analysis carried out with the specified number of EOFs. The symbols ∗ (○) mark significant correlations at a significance level of 99% (95%).

yields a pronounced ridge over western Europe and a weakened northwesterly flow over the Alps. This pattern is connected with negative precipitation anomalies at each station. The patterns describe 31% and 48% of the variability of the geopotential field and the precipitation field, respectively, and have a canonical correlation of 0.88 (Table 2).

The 2nd pair of patterns (Fig. 2) displays an anomalous meridional flow that is associated with mainly positive precipitation anomalies on the windward side and negative anomalies on the leeside of the Alps. A strengthened northwesterly flow over the British Isles and middle Europe is connected with strong negative precipitation anomalies in the south and mainly positive anomalies north of the Alps. These patterns explain 20% and 16% of the variance of the geopotential field and of the precipitation field, respectively. The canonical correlation between the 2 fields is 0.74 (Table 2). The 3rd pair of patterns (not shown) describes a high pressure cell over mid Europe which is connected with an anomalous northwesterly flow over northern Europe. This pressure pattern is associated with negative precipitation anomalies in the south and east of the Alps and minimal anomalies at the rest of the stations. The canonical correlation is only 0.13.

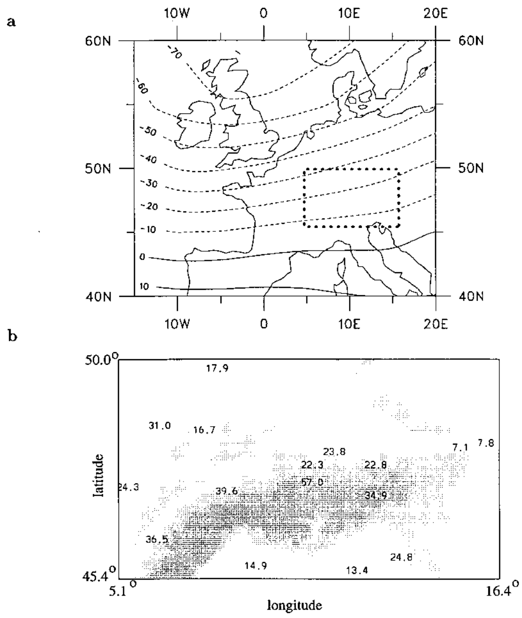

Fig. 1. First pair of canonical correlation patterns of the first half of the time series of the geopotential and the precipitation data a geopotential pattern (in gpm) and **b** precipitation pattern (in mm/month) at 16 stations in or close to the Alps. Orographic heights over 600 m are shaded, with an increment between levels of 400 m. The box in (a) indicates the area shown in (b).

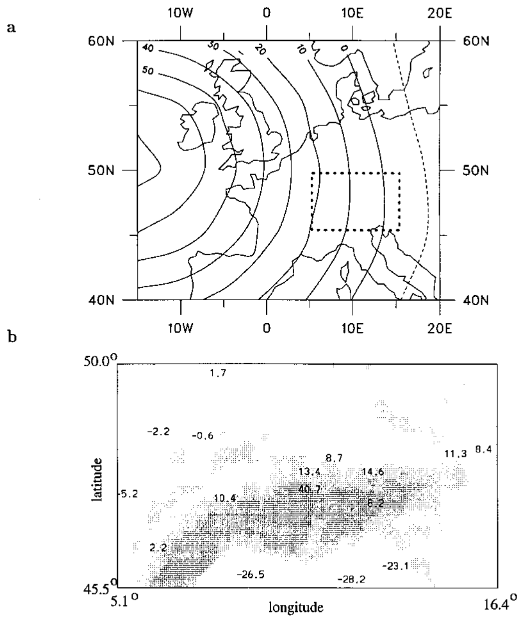

Fig. 2. As in Fig. 1 but for the second canonical correlation patterns of the 1st half of the time series.

The EOF-analysis and the CCA has been repeated for the 2nd part of the data set and compared to the results of the analysis of the 1st half of the data set. The analysis of the 2nd half of the time series yields only slightly modified results. In order to obtain a measure of the similarity of the pairs of CCA-patterns the time series of the respective geopotential patterns have been calculated for the whole time series by projecting the geopotential field onto the patterns. Then the time series were correlated. The pair of patterns which has the highest canonical correlation in the 2nd half of the data set is similar to the 2nd pair of patterns of the 1st half of the data set and the time series of their geopotential patterns have a correlation of 0.79 (Table 3). The 1st canonical precipitation pattern for the 2nd half of the time series explains about 5% more variance than the corresponding pattern for the 1st half of the time series. The 2nd pair of canonical correlation patterns for the 2nd half of the time series resembles the 1st pair of patterns for the 1st half of the time series and the time series of their geopotential patterns have a correlation of 0.91 (Table 3). However, the geopotential pattern has a stronger meridional component and the precipitation pattern explains slightly less variance (about 4% less) than the corresponding pattern for the 1st half of the time series. The 3rd pairs of canonical correlation patterns resulting from the analysis of the respective halfs of the time series

Table 3. *Correlation of the time series of the canonical correlation patterns of the geopotential height of the analysis of the 1st half of the time series (top to bottom) and the 2nd half of the time series (left to right).*

CCA-pattern 1.H.↓ 2.H.→	1	2	3
1	0.28	0.91	−0.42
2	0.79	−0.46	−0.26
3	−0.40	−0.37	−0.82

The complete data set of the geopotential field is projected onto the geopotential patterns of both analyses and the resulting time series are correlated over the whole time period.

are very similar. The correlation of the two time series of the geopotential patterns is 0.82 (Table 3).

Very similar relationships were also obtained in an analysis with a spatially much larger 500 hPa geopotential height field (Burkhardt, 1995) reflecting again the stability of the results of the CCA.

4. Regression model and its validation

A set of multivariate regression models is constructed based on the results of the CCA of one half of the observational data (eq. (2)), and validated on the other half of the data. The multivariate regression models are based on the results of the CCA described in the previous Section and use 1, 2 or 3 pairs of canonical correlation patterns. The observed geopotential field serves as input for the model from which an associated precipitation field is calculated. For the purpose of model validation this estimated precipitation field is then compared with the observed precipitation. The application of the regression model to the half of the data set for which the CCA was carried out yields the hindcast skill and to the independent half of the time series the forecast skill of the model (Table 4).

The models using 1, 2 and 3 pairs of canonical correlation patterns of the analysis of the 1st half of the time series have an overall hindcast skill (eq. (3)) of 36.4, 49.3 and 49.4 and an overall forecast skill of 27.6, 45.6 and 46.6 (eq. (3)), respectively (Table 4). The overall skill measures the performance of the models in simulating the mean precipitation anomaly at the stations. The forecast skill of the model using one pair of patterns is much smaller than the hindcast skill since the associated precipitation pattern describes much less variance in the 2nd half than in the 1st half of the time series. On the other hand, the anomalous meridional flow (2nd pair of patterns) is more important for the precipitation in the 2nd half of the time series as seen in the results of the CCA. This corresponds to a higher percentage of precipitation variance being inferred from the variability of the meridional flow in the 2nd half of the time series than in the 1st half.

Regression models set up using the analysis of the 2nd half of the time series have a higher hindcast skill and a slightly lower forecast skill than the models based on the results of the CCA of the 1st half of the time series. As an additional test, regression models based on a CCA using more time series than those of the 1st 3 geopoten-

Table 4. *Hindcast skill and forecast skill of the regression model at individual stations and for the overall model.*

	Hindcast skill			Forecast skill		
Stations	1	2	3	1	2	3
Nancy	70.0	70.1	69.7	53.2	53.0	53.6
Strasbourg	53.5	54.3	53.5	39.2	39.0	38.7
Dijon	53.3	53.2	53.2	31.5	38.3	38.6
Geisenheim	45.2	49.8	48.7	39.9	37.7	37.1
München	48.2	52.1	52.0	30.2	33.8	33.3
Zugspitze	33.4	55.8	55.6	34.6	62.4	64.8
St. Pölten	6.0	23.3	26.5	11.1	9.8	9.6
Wien	10.4	23.5	23.7	17.3	25.1	25.6
Sonnenblick	31.2	35.5	35.1	43.8	50.1	51.5
Salzburg	32.9	40.5	40.4	22.7	29.8	28.0
Milano	9.7	43.2	43.4	−13.9	37.9	39.9
Venezia	14.3	41.3	42.0	−15.2	36.7	39.8
Trieste	31.5	45.7	45.1	5.8	36.3	38.6
Hohenp.berg	33.7	40.4	40.1	37.3	41.7	40.7
Zürich	64.0	66.6	66.9	45.1	40.9	39.8
Geneve	50.6	49.4	49.6	32.3	27.3	25.1
Overall	36.4	49.3	49.4	27.6	45.6	46.6

The model was constructed using 1, 2 or 3 pairs of patterns of the CCA of the first half of the time series.

tial and the 1st 4 precipitation EOFs were constructed. Those models have only a slightly higher hindcast skill. On the whole, the models are relatively stable against changes in the analysis period.

The skill of the models and the importance of the geopotential patterns for the precipitation variability is very different at each station. Negative values indicate a higher variance of the error of the estimated precipitation anomaly than the variance of the precipitation anomaly itself. The precipitation at the western stations, that is the French, Swiss and German stations, is well simulated by the model which is based on the CCA of the 1st half of the time series and which uses only the 1st pair of canonical correlation patterns. This means that the westerly flow is the dominant predictor pattern for the precipitation at these stations. However, the model consisting of only the 1st pair of canonical correlation patterns has a very low hindcast and a negative forecast skill at the southern stations. The use of the 2nd pair of canonical correlation patterns, which describes the dependence of the precipitation on the meridional flow anomaly greatly improves the performance of the statistical model, especially at the Italian stations. The inclusion of the 3rd pair of patterns increases the skill only very slightly. The precipitation variance described at the Austrian stations is generally very low. The forecast skill of the overall model is higher than the forecast skill at most of the stations. This is caused by the high skill at those stations which have a very high precipitation variability and therefore influence the overall skill strongly.

Fig. 3a shows the time series of the observed and simulated precipitation anomaly averaged over the French, Swiss and German stations. For the simulation the multivariate regression model based on the 1st 2 pairs of canonical correlation patterns of the 1st half of the time series was used. The 3rd pair of patterns was not included in the regression model since it did not increase the skill significantly. Both this model and the model based on the analysis of the 2nd half of the time series have problems reproducing the mean precipitation at the French, Swiss and German stations during the period 1978–80. In this particular time, the 500 hPa geopotential height field has a strong meridional anomaly and the westerly component is relatively weak. Accordingly, the precipitation at this time is simulated poorly at the northwestern stations and relatively well at the Italian stations (Fig. 3b). In the years in which the precipitation at the northwestern stations is simulated very well (1965 to 1972), the precipitation at the Italian stations is poorly simulated. This indicates the tendency to simulate either the Italian stations or the northwestern stations well, depending on the amplitude of the geopotential patterns. Fig. 3c shows the corresponding time series of the precipitation anomaly at the Austrian stations. Although the skill of the model in simulating the monthly precipitation anomalies at the Austrian stations is very low, the long term variability of the precipitation is simulated relatively successfully except in the time around 1980. Overall the model simulates the long term variability of the precipitation well, as far as this can be examined on the basis of a time series of only 35 years.

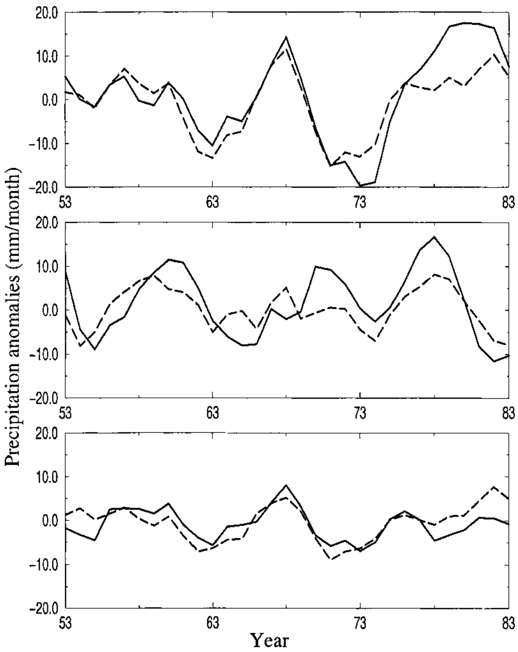

Fig. 3. Time series of observed (solid lines) and simulated (dashed lines) precipitation anomalies (in mm/month) at (a) the stations north and west of the Alps, (b) the Italian stations and (c) the Austrian stations. The time series are smoothed with a 5-year running mean. The regression model is based on the first two pairs of correlation patterns of the first half of the time series.

5. Precipitation in a tripled CO_2-climate

Before applying the statistical model to the 500 hPa geopotential height field simulated by a GCM for an increased CO_2 concentration, the realism of the geopotential field simulated by the GCM must be examined. Roeckner et al. (1992) examined the simulation of the large scale geopotential field and found that the ECHAM3-model simulates this field fairly well. Ponater et al. (1994) found that even the older ECHAM2 model version simulates the interannual variability of the large scale geopotential realistically. In this paper the simulation of the geopotential shall only be validated in terms of its main variability patterns (EOFs). The variability patterns are of special importance because the precipitation change in the area of the Alps must be inferred from the change in the large scale geopotential simulated by the GCM.

The spatial fields of the main variability patterns (EOFs) of the geopotential field simulated by the GCM for $1 \times CO_2$ and for $3 \times CO_2$ conditions are nearly identical with those of the observational data. The variance described by those EOFs varies slightly. Table 5 lists the amount of variance described by the EOFs of the two model simulations and the amount of variance of the modeled geopotential fields described by the EOFs of the observed geopotential field. The latter was calculated by projecting the simulated fields onto the EOFs of the observed geopotential field. The 1st EOF of the observational data explains more variance of the simulated geopotential field ($1 \times CO_2$) than of the observational data, whereas the 2nd and 3rd EOFs explain nearly the same and a smaller percentage of the simulated geopotential variance ($1 \times CO_2$), respectively, compared with the observational data. This means that the variability of the geopotential pattern, describing positive (negative) anomalies in the whole analysed area is significantly overestimated by the model whereas the variability of the west-east gradient of the geopotential might be slightly underestimated.

Table 5. *Variance described by the EOFs of the observed geopotential field and the geopotential fields simulated by the GCM for $1 \times CO_2$- and $3 \times CO_2$-conditions (%).*

No. EOFs	1	2	3	4	5
EOFs 500 hPa	47.9	23.9	18.3	4.8	2.8
EOFs $1 \times CO_2$ exp.	54.1	24.1	16.6	2.8	1.3
EOFs $3 \times CO_2$ exp.	60.1	25.0	9.1	3.4	1.4
projection $1 \times CO_2$ exp.	53.6	23.6	16.7	2.3	1.2
projection $3 \times CO_2$ exp.	59.2	22.4	10.7	2.9	1.5

Overall the variability patterns of the observed large scale geopotential field are reasonably well reproduced by the GCM. The difference in explained variance between the $1 \times CO_2$ and $3 \times CO_2$ simulations is largest for the 1st and the 3rd EOF reducing the percentage of the variability described by the zonal geopotential gradient in the $3 \times CO_2$ simulations by 1/3.

The difference of the time mean northern hemispheric geopotential field simulated by the GCM for a $3 \times CO_2$ and $1 \times CO_2$ concentration is shown in Fig. 4. The GCM simulates an increased height of the 500 hPa level globally and an enhanced southwesterly flow component over Europe in the $3 \times CO_2$ simulation. This pattern can not be reconstructed using the EOFs and hence the geopotential predictor patterns of the regression model. The statistical model is therefore applied to the change in geopotential after a subtraction of the average over the whole area. This is justifiable since the effect of a rise in humidity which may be connected with the general rise in geopotential height which in turn is connected with a rise in temperature can not be simulated by the present statistical model in any case. A general increase

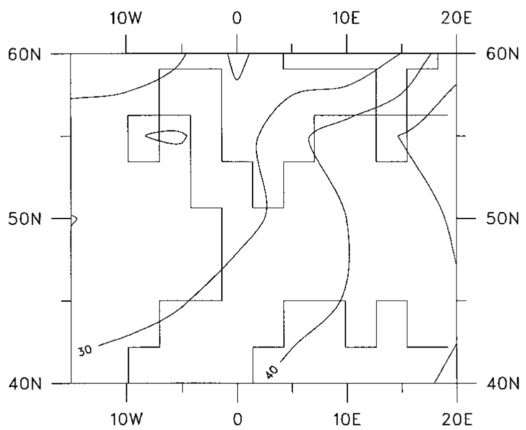

Fig. 4. Difference of the time mean geopotential field between the GCM simulations of a $3 \times CO_2$- and a $1 \times CO_2$-climate (in gpm). The European coastline is also shown at the GCM resolution.

of the height of the 500 hPa level over the whole northern hemisphere, on the other hand, does not cause changes in the general circulation such as changes in the flow regimes or changes in the location of the storm tracks.

The geopotential field is very well resolved by the EOFs after subtraction of the area average. Calculating the amplitudes of the geopotential patterns ($v^{(i)}$ in eq. (1)), the largest amplitude is obtained for the geopotential pattern of the 3rd pair of canonical correlation patterns and the 2nd highest for the geopotential pattern of the 2nd pair. This means that the largest part of the geopotential change pattern simulated by the GCM can be described by a pattern which was found in observational data to be only marginally correlated with the precipitation anomalies in the area of the Alps and which was therefore not included in the statistical model. In Fig. 5 the geopotential change pattern as resolved by the statistical model, based on the 1st 2 pairs of canonical correlation patterns, is shown. The part of the geopotential change pattern resembling the west-east gradient is resolved, but the gradient is quite weak. The precipitation changes associated with the geopotential change resolved by the statistical model (Fig. 5) are shown in Fig. 6. The statistical model yields an increase in precipitation at the stations south and west of the Alps with

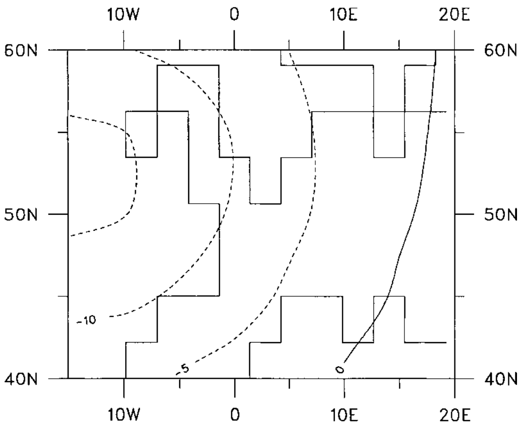

Fig. 5. Reconstruction of the geopotential field simulated by the GCM, as resolved by the statistical model (in gpm) using the first two geopotential predictor patterns. The area mean change of the geopotential was subtracted before applying the statistical model. Also shown is the European coastline at the GCM resolution.

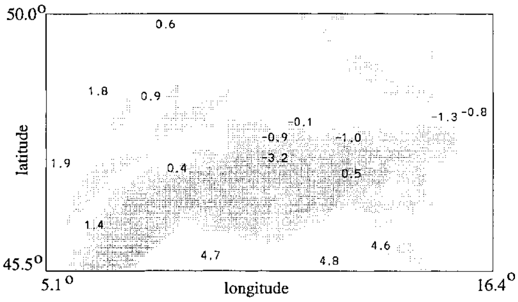

Fig. 6. Change in precipitation at 16 Alpine stations due to a tripling of the CO_2-concentrations (in mm/month). The precipitation change was obtained by applying a statistical model to the change of the geopotential field simulated by an GCM. Orographic heights over 600 m are shaded, with an increment between levels of 400 m.

maximal changes at the Italian stations. At the stations in the northeast of the Alps the precipitation would decrease due to a tripling of the CO_2 concentration. The precipitation changes range from 0% to 8% of the monthly mean precipitation. The highest percentage change is obtained for the Italian stations (6% to 8%) and the 2nd highest for the French stations (around 3%). For the other northwestern stations an increase in precipitation between 0% and 2% and for the northern and northeastern stations a slight decrease of up to 3% of the monthly mean precipitation is obtained.

The precipitation change estimated by the statistical model varies only very slightly when changes in the statistical model are introduced. Several statistical models were constructed using the results of the CCA (Table 2) which were conducted with varying number of EOFs retained. The models were applied to the geopotential field (Fig. 4) with prior subtraction of the area average. The calculated precipitation change turned out to be least dependent on the statistical model at the stations west and north of the Alps. There the difference in precipitation change ranges between less than 0.1 mm/month and 0.3 mm/month. At the stations south of the Alps and in the Alps the differences in the precipitation change, calculated by the statistical models, amounts to up to 1.4 mm/month.

It is of interest to compare the change in Alpine precipitation simulated directly by the GCM with that inferred from the large scale GCM simulations by the statistical model. In Fig. 7 the differ-

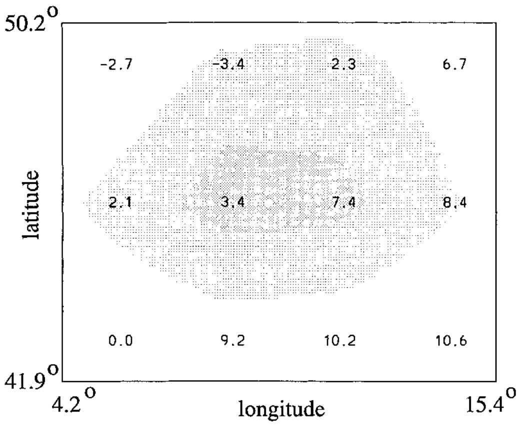

Fig. 7. Difference of the time mean precipitation field between a $3 \times CO_2$-simulation and a $1 \times CO_2$-simulation (in mm/month) and 'Alpine' orography of the GCM. Orographic heights over 600 m are shaded, with an increment between levels of 200 m.

ence between the winterly precipitation in the $3 \times CO_2$-climate and in the $1 \times CO_2$-climate simulated by the GCM is shown. The GCM simulates an increase in precipitation in the Alpine area except in the northwest of the "model-Alps" for $3 \times CO_2$-conditions. South of the Alps the change ranges from 15% to 35% of the monthly mean precipitation and decreases towards the north (where the change is between 2% and 5%). The decrease in precipitation in the northwest is about 15%.

The differences between the precipitation changes simulated by the GCM directly and inferred by the statistical model may partly be due to the simplified orography in the GCM which misrepresents the flow around the Alps. Another reason for the larger precipitation changes simulated by the GCM may be that the connection between the precipitation field in the area of the "model-Alps" and the geopotential field is overestimated by the GCM (Burkhardt, 1995). This means that changes in the large scale flow cause higher precipitation changes in the GCM than in nature. Another possible reason may be that in a future climate this relationship may have a changed importance for the Alpine precipitation or the relationship itself may change. Furthermore, the statistical model simulates only the precipitation anomalies which are associated with the variability of the large scale flow, and describes only about 50% of the observed precipitation variance. The precipitation changes simulated by the GCM on the other hand are not only due to the changed large scale flow, but are very likely to be influenced by factors such as an increase of water vapour in the atmosphere.

6. Conclusions

A statistical model is constructed in order to estimate the change of winter time Alpine precipitation due to a tripling of the CO_2 concentration from the large scale simulation of a GCM. A good predictor for the Alpine precipitation was found to be the 500 hPa height field. The statistical model consists of physically plausible statistical relationships between the 500 hPa geopotential height field and the Alpine precipitation field found in observational data, which describe the dependence of the Alpine precipitation on the strength of the westerly flow and on the strength of the meridional flow component. These relationships are used to determine quantitatively the expected change in the precipitation field from the change of the large scale 500 hPa geopotential change simulated by the GCM.

The statistical model describes about 50% of the Alpine precipitation variance in an independent data set and captures the long term variability of the precipitation well. The model is very stable with respect to changes in the analysis period and the particular choice of the number of EOFs included in the model. The skill of the model varies considerably between the different stations. For the precipitation variance at the stations west and north of the Alps the strength of the westerly flow is most important, whereas at the southern stations the influence of the meridional flow dominates. At times when the meridional flow anomalies are strongest the precipitation at the southern stations is simulated well, and at times when the westerly flow anomaly is strongest the precipitation at the stations in the north and west of the Alps is simulated well. Overall, the model is reasonably successful in reproducing the long term variability of the precipitation.

The statistical model is able to resolve the change in the 500 hPa geopotential height field simulated by the GCM for a tripled CO_2 concentration well, as long as the area average of the geopotential change is subtracted beforehand. The precipitation change obtained from the statistical model for the winter months is greatest at the southern stations where the increase amounts to between 6 and 8% of the monthly mean precipitation. In the north and west of the Alps a smaller increase is obtained. The estimated precipitation change depends only slightly on the details of the statistical model, i.e., on the choice of the number of EOFs used in the CCA. As seen in the verification period, the precipitation obtained by the statistical model from a meridional flow anomaly is very reliable at the southern stations and slightly less reliable at the northern and western stations. Therefore the precipitation change obtained by the statistical model for the southern stations may be the most robust feature.

The precipitation change estimated in this study for an increasing CO_2 concentration agrees quite well with the qualitative change of the Alpine precipitation estimated by a mesoscale model coupled statistically with a GCM (Frey-Buness et al., 1995). Frey-Buness et al. finds an increase of precipitation in the whole Alpine area with a maximal increase south west of the Alps. Quantitative estimates were not made by these authors.

There are 2 studies which simulate a change in Alpine climate due to a doubling of the CO_2 concentration using a nested model (Giorgi et al., 1992; Jones et al., 1997). The increase of Alpine wintertime precipitation obtained by Giorgi et al. seems to be slightly smaller than the change estimated in this study for a tripling of the CO_2 concentration. But the estimation of Giorgi et al. (1992) is based on the results of only 5 single months, so that the estimate can not be expected to be very reliable. The results of Jones et al. (1997) are qualitatively similar to the change of Alpine precipitation estimated here. But they obtain a much larger change in Alpine wintertime precipitation for $2 \times CO_2$ conditions than estimated here with an maximum increase south of the Alps of about 30 mm/month. A more thorough comparison between the change in the precipitation field simulated by Giorgi et al. and Jones et al. for $2 \times CO_2$ conditions and the change at the single stations obtained here for $3 \times CO_2$ conditions is not possible because of the relatively coarse resolution of their climate change estimates. Slight differences between the precipitation change estimated here and those obtained from nested model studies may represent agreement since the model used here does not include all the factors causing a change in Alpine precipitation.

The estimation of the change of Alpine precipitation due to a doubling of the CO_2 concentration by Gyalistras et al. (1994) which was obtained using a similar method to the method used in this study gives a much higher precipitation change than estimated here (up to 50% of the monthly mean precipitation). This disagreement is likely to be caused by several reasons. One reason may be that Gyalistras et al. applied the statistical model to the large scale fields of surface pressure and temperature without subtraction of the area mean which could mean that the predictor field is not captured properly by the statistical model. Another reason could be the low skill of the part of the model of Gyalistras et al. which is related to the precipitation change. Furthermore and probably most important, the change of Alpine climate due to a change in the CO_2 concentration is inferred from the change of the surface pressure and temperature field simulated by an older, low resolution version (ECHAM1/T21) of the GCM used here (ECHAM3/T42). This older model version is known to be less successful in the simulation of the present large scale climate (Roeckner et al., 1992) and simulates a very different change of the geopotential field for a tripling of the CO_2 concentration than the newer model version (Perlwitz, personal communication). This difference in the simulated large scale changes would have a much bigger impact on the small scale precipitation change than the uncertainty associated with changes in the set up of the statistical model.

All the different studies compared above predict a qualitatively similar change of Alpine precipitation due to an increase in the CO_2 concentration. Quantitatively though, the predictions vary greatly. The fact that the study which uses the most similar methodology obtaines the most different change in Alpine precipitation suggests that a large, if not the largest, error is introduced by the large scale simulations of the climate models which are used by all regionalisation methods as input. As long as the diversity of large scale model predictions by different climate models or climate model versions remains, any estimate of the spatial structure of climate change should be viewed with caution.

7. Acknowledgements

I would like to thank the MPI Hamburg for making the model simulations available. Thanks especially to Jan Perlwitz for information regarding the time slice experiment. I would like to also thank Professor Werner Metz and Prof. Joseph Egger for stimulating this work. Furthermore, thanks are due to Dr. Eduardo Zorita for many helpful discussions. The paper was improved by the comments of three anonymous referees. This work was supported by the grant "Dynamische Analyse regionaler Klimaänderungen" from the Bavarian Climate Research Programme BayFORKLIM.

REFERENCES

Anderson, T.W. 1984. *An introduction to multivariate statistical analysis*. Wiley series in Probability and Mathematical Statistics, 675 pp.

Bardossy, A. and E. J. Plate, 1992. Space-time model for daily rainfall using atmospheric circulation patterns. *Water Resources Res.* **28**, 1247–1259.

Barnett, T. and R. Preisendorfer, 1987. Origins and levels of monthly and seasonal forecasts skill for United States surface air temperatures determined by canonical correlation analysis. *Mon. Wea. Rev.* **115**, 1825–1850.

Boer, G. J., K. Arpe, M. Blackburn, M. Deque, W. L. Gates, T. L. Hart, H. Le Treut, E. Roeckner, D. A. Sheinin, I. Simmonds, R. N. B. Smith, T. Tokioka, R. T. Wetherald and D. Williamson, 1992. Some results from an intercomparison of the climates simulated by 14 atmospheric general circulation models. *J. Geophys. Res.* **97**, 12771–12786.

Bretherton, C. S., C. Smith and J. M. Wallace,1992. An intercomparison of methods for finding coupled patterns in climate data. *J. Clim.* **5**, 541–560.

Burkhardt, U. 1995. Validation of the small-scale performance of a climate model. *Clim. Dyn.* **11**, 299–305.

Cubasch, U., K. Hasselmann, H. Höck, E. Maier-Reimer, U. Mikolajewicz, B. D. Santer and R. Sausen, 1992. Time-dependent greenhouse warming computations with a coupled ocean-atmosphere model. *Clim. Dyn.* **8**, 55–69.

Cubasch, U., H. Von Storch, J. Waszkewitz and E. Zorita, 1996. Estimates of climate change in Southern Europe derived from dynamical climate model output. *Clim. Res.* **7**, 129–149.

DKRZ, Modellbetreuungsgruppe, 1994. The ECHAM3 atmospheric general circulation model. *DKRZ, Technical Report* **6**, 182pp.

Egger, J. 1995. Regional statistical-dynamical climate modelling. Tests. *Beitr. Phys. Atmosph.* **68**, 281–289.

Frey-Buness, A., D. Heimann and R. Sausen, 1995. A statistical-dynamical downscaling procedure for global climate simulations. *Theor. Appl. Climatol.* **50**, 117–131.

Giorgi, F. 1990. Simulation of regional climate using a limited area model nested in a general circulation model. *J. Clim.* **3**, 941–963.

Giorgi, F., M. R. Marinucci and G. Visconti, 1990. Use of a limited-area model nested in a general circulation model for regional climate simulation over Europe. *J. Geophys. Res.* **95**, 18413–18431.

Giorgi, F. and L. O. Mearns, 1991. Approaches to the simulation of regional climate change. a review. *Rev. Geophys.* **29**, 2, 191–216.

Giorgi, F., M. R. Marinucci and G. Visconti, 1992. A $2 \times CO_2$ climate change scenario over Europe generated using a limited area model nested in a general circulation model 2. climate change scenario. *J. Geophys. Res.* **97**, 10011–10028.

Grotch, S. L. and M. C. MacCracken, 1991. The use of general circulation models to predict regional climatic change. J. Climate, **4**, 286–303.

Gyalistras, D., H. Von Storch, A. Fischlin and M. Beniston, 1994. Linking GCM-simulated climatic changes to ecosystem models: case studies of statistical downscaling in the Alps. *Clim. Res.* **4**, 167–189.

Hewitson, B. C. and Crane, 1992. Regional Climates in the GISS global circulation model: synoptic-scale circulation. *J. Climate* **5**, 1002–1011.

Hughes, J. P., D. P. Lettenmaier and P. Guttorp, 1993. A stochastic approach for assessing the effect of changes in synoptic circulation patterns on gauge precipitation. *Water Resour. Res.* **29**, 3303–3315.

Jones, R. G., J. M. Murphy, M. Noguer and A. B. Keen, 1997. Simulation of climate change over Europe using a nested regional-climate model. II. Comparison of driving and regional model responses to a doubling of carbon dioxide. *Q.J.R. Meteorol. Soc.* **123**, 265–292.

Karl, T. R., W.-C. Wang, M. E. Schlesinger, R. W. Knight and D. Protman, 1990. A method of relating general circulation model simulated climate to the observed local climate. Part I. Seasonal statistics. *J. Clim.* **3**, 1053–1079.

Kim, J.-W., J.-T. Chang, N. L. Baker, D. S. Wilks and W. L. Gates, 1984. The statistical problem of climate inversion: determination of the relationship between local and large-scale climate. *Mon. Weather Rev.* **112**, 2069–2077.

Machenhauer, B., M. Windelband, M. Botzet, R. G. Jones and M. Deque, 1996. Validation of present-day regional climate simulations over Europe. Nested LAM and variable resolution global model simulations with observed or mixed layer ocean boundary conditions. *MPI für Meteorologie, Report 191,* 60 pp.

Marinucci, M. R. and F. Giorgi, 1992. A $2 \times CO_2$ climate change scenario over Europe generated using a limited area model nested in a general circulation model 1. present-day seasonal climate simulation. *J. Geophys. Res.* **97**, 9989–10009.

Marinucci, M. R., F. Giorgi, M. Beniston, M. Wild, P. Tschuck, A. Ohmura and A. Bernasconi, 1994. High resolution simulations of January and July climate over the western Alpine region with a nested regional model system. *Theor. Appl. Climatol.* **51**, 119–138.

McGinnis, D.L. 1997. Estimating Climate-Change Impacts on Colorado Plateau Snowpack Using Downscaling Methods. *Professional Geographer* **49**, 117–125.

Metz, W. 1991. Optimal relationship of large-scale flow patterns and the barotropic feedback due to high-frequency eddies. *J. Atmos. Sci.* **48**, 1141–1159.

Perlwitz, J., U. Cubasch and E. Roeckner, 1992. Simulation of greenhouse warming in the ECHAM-3 model using the time-slice method. In G.J. Boer (ed.). Research activities in atmospheric and oceanic modelling, *CAS/JSC Working Group on Numerical Experimentation, Report No. 19, WMO/TD-No. 592,* 9.3–9.4.

Ponater, M., W. König, R. Sausen and F. Sielmann, 1994. Circulation regime fluctuations and their effect on intraseasonal variability in the ECHAM climate model. *Tellus* **46A**, 265–285.

Preisendorfer, R. W. 1988. *Principle Component Analysis in Meteorology and Oceanography, Developments in Atmospheric Science* **17**, Elsevier, 425 pp.

Roeckner, E., K. Arpe, L. Bengtsson, S. Brinkop, L. Dümenil, M. Esch, E. Kirk, F. Lunkeit, M. Ponater, B. Rockel, R. Sausen, U. Schlese, S. Schubert and M. Windelband, 1992. Simulation of the present-day climate with the ECHAM model. impact of model physics and resolution. *MPI für Meteorologie, Report 93,* 172pp.

Saunders, I. R. and J. M. Byrne, 1996. Generating regional precipitation from observed and GCM synoptic-scale pressure fields, southern Alberta, Canada. *Clim. Res.* **6**, 237–249.

Von Storch, H., E. Zorita and U. Cubasch, 1993. Downscaling of global climate change estimates to regional scales: an application to Iberian rainfall in wintertime.*J. Climate* **6**, 1161–1171.

Wilks, D. S. 1995. *Statistical methods in the atmospheric sciences.* Academic Press, 464pp.